Available online at www.sciencedirect.com

ScienceDirect

Procedia CIRP 124 (2024) 135–140

www.elsevier.com/locate/procedia

13th CIRP Conference on Photonic Technologies [LANE 2024], 15-19 September 2024, Fürth, Germany

Comparison of in-process laser drying with furnace and vacuum drying to reduce moisture of AlSi10Mg powder processed in Laser Powder Bed Fusion

Victor Lubkowitz[a,*], Leonie Fayner[a], Steffen Kramer[b], Volker Schulze[a], Frederik Zanger[a]

[a]*Institute of Production Science (wbk), Karlsruhe Institute of Technology (KIT), Kaiserstraße 12, 76131 Karlsruhe, Germany*
[b]*Institut fuer Strahlwerkzeuge (IFSW), University of Stuttgart, Pfaffenwaldring 43, 70569 Stuttgart, Germany*

* Corresponding author. Tel.: +49 721 608 44288. *E-mail address:* victor.lubkowitz@kit.edu

Abstract

In most powder bed-based laser melting systems (PBF-LB), metal powders must be handled without inertization but in an air atmosphere for a short time, increasing the AlSi10Mg powder moisture and reducing the achievable component density. Consequently, different drying methods were investigated. Drying in a furnace with an inert atmosphere, using a vacuum to evaporate the water at low temperatures, and vaporizing moisture layerwise from the spreaded powder with a defocused, low-power laser beam as a further process step of the PBF-LB process. Therefore, four different moisturized powders, which were dried with different settings for the drying methods, are analyzed. All drying methods reduce the moisture content of the powder, with in-process drying being the most effective. Due to the oxide layer growth around the particles during furnace and vacuum drying, the achievable sample density after drying is worse. In-process drying with low energy density is the best option to reach a reduction of hydrogen pores and an increase of density.

Keywords: PBF-LB, AlSi10Mg; powder moisture; laser drying; vacuum drying; furnace drying

1. Introduction

AlSi10Mg is widely used to produce powder bed-based selective laser melting (PBF-LB) parts. The mechanical properties of the parts are strongly influenced by the achieved density [1,2]. Fully dense material has not yet been achieved in this process. Many publications discussed the influence of the process parameters on process pores when the material is superheated and a deep keyhole collapse [3–5] or lack of fusion (LoF) pores when the energy input is too low for a complete melting of the powder layer [6]. Optimization of the process parameters allows the part production with a minimum rest porosity of about 0.04 % [7]. However, in many investigations only fresh powder material was used. In industrial applications powder materials are often sieved and reused due to resource efficiency and their high costs. Depending on the machine setup and degree of industrialization, the powder materials get in contact with the air atmosphere when the remaining powder is removed from the build chamber and the powder is sieved or stored. Weiss et al. showed that especially AlSi10Mg powder moisture strongly increases when it comes in contact with air humidity, which results in a substantial density decrease, also when adjusting the process variables [8]. Li et al. proved that AlSi12 powder drying in an air atmosphere at 100 °C for up to 60 min increases the part density as less oxygen from the water is available to form Al-oxides and -hydroxides, which negatively influence the density and result in pore formation [9]. Weingarten et al. introduced an additional process step to the PBF-LB process, by first laser drying the AlSi10Mg powder with a low laser power of 50 W before melting it and

10.1016/j.procir.2024.08.086

compared this method with furnace drying with up to 200 °C. Both methods reduced the hydrogen pore density as less hydrogen is absorbed in the melt, which forms pores if the local solubility limit of the melt is reached [10]. Irrespective of the melting process, Cordova et al. proved the powder recoatability of AlSi10Mg powder when vacuum or furnace-dried compared with moisturized powder. They found that the highest powder bed density can be achieved by furnace drying, but all powder conditions were recoatable [11].

The negative influence of moisture on the PBF-LB process has been sufficiently investigated. Research has also presented various approaches (furnace, vacuum, and laser drying) to reduce the moisture in metal powders to increase the components' density. However, a direct comparison of the three drying methods and their impact on resulting part density is missing. In order to accomplish with this deficit, AlSi10Mg powder with different moisture content is dried using the above-mentioned methods. The remaining moisture is analyzed by Karl Fischer titration (KFT), and the resulting component density and hydrogen pore content are determined.

2. Materials and Methods

2.1. Powder conditioning and drying methods

Before and after a drying method, the powder moisture of all powder conditions was measured via Karl Fischer titration (KFT) by m4p material Solutions GmbH (Feistritz im Rosental, Austria).

The AlSi10Mg powder (d_{10}: 28.83/d_{50}: 41.88/d_{90}: 55.64 µm, camsizer analysis) was purchased from m4p material Solutions GmbH (Magdeburg, Germany). The various investigated powder conditions were set in an Agilis 600 l climatic chamber from RS-Simultoren Prüf- und Messtechnik GmbH (Oberhausen, Germany). The powder was conditioned for 72 h at 25 °C at a relative humidity of 50 % or 50 °C and 80 %, respectively. After wetting, the powder cooled back to room temperature and was sieved using a 63 µm laboratory sieve AS 200 Control from Retsch GmbH (Haan, Germany) to break up the formed lumps, which result from liquid necks due to the capillary effect [12]. Further new material (vacuum sealing opened directly before experiments) and stored material were investigated.

Furnace drying was done in a tube furnace GLO 10/11-2G from Carbolite Gero GmbH & Co. KG (Neuhausen, Germany). 0.5 kg of powder material was placed in a stainless steel bowl for each drying temperature. A vacuum was applied to the furnace chamber for 5 minutes and the chamber was flooded with argon gas to prevent the powder from oxidation during heating. The heating rate was 10 K/min, and the holding time was 60 min. After cooling, the powder was packed in laboratory glassware.

Vacuum drying was carried out at AMproved GmbH (Bad Lippspringe, Germany) with the drying module AM1000. Therefore, 0.75 kg powder was filled in 4 l stainless steel bottles from the same company. Two different drying process sequences were investigated. Drying took place in repeated cycles. First, a negative relative pressure was applied and hold for 60-600 s to evaporate water at room temperature (26.4 mPa absolute at 22 °C [13]). After that, the bottle was flooded with argon gas.

For laser drying the Gaussian laser beam (wavelength 1070 nm, $M^2 \sim 1{,}3$) was defocused by shifting the focal plane 10 mm above the powder layer to achieve a larger spot diameter and lower the intensity in the beam center to prevent the irradiated area from melting. Further, the diameter of the dried surface is 1 mm larger than the melted sample cross-section. For the production of powder samples for the KFT analysis of the in-process drying five complete layers were exposed without melting and extracted from the build chamber.

All described drying methods to set the different powder conditions are summarized in table 1.

Table 1: Overview of all powder conditions and drying process settings

powder conditions temp. (°C)/ rel. humidity (%)	**furnace drying** temp. (°C)	**vacuum drying** name/minimum pressure (mPa)/holding time (s)/cycles	**in process drying** power (W)/ velocity (mm/s)/ hatch distance (mm)/ EV(J/mm^3)
new	80	V5/25 /600/5	75/1500/0.155/6.5
stored	120	V20/80/60/20	75/1000/0.155/9.7
25/50	160		25/1037/0.16/3.0
50/80	200		39/1288/0.155/3.9

2.2. Specimen production and analysis

An SLM280HL machine was used for the experiments, equipped with a ytterbium fiber laser from IPG. The beam has a Rayleigh length of z_R= 3.57 mm and a spot size of w_0= 81 µm. The layer thickness was 50 µm. The build chamber is flooded with argon until less than 100 ppm of remaining oxygen to avoid oxidation effects. A self-designed platform reduction with a diameter of 100 mm and a special recoater were used, to operate the machine with small amounts of powder.

The samples had a diameter of 11 mm and a height of 11 mm. The samples were manufactured with a laser power of 350 W, a hatch distance of 0.17 mm, and a variable scan speed of 950/1150/1350 mm/s. 4 to 6 samples were manufactured for each speed to ensure statistical validation.

After production, the specimens were cut off the building platform by wire arc EDM, and the side surface was captured using a VHX-7000 microscope from Keyence. Further, the side surface roughness was measured once at every specimen with a Nanofocus µSurf 800-L from NanoFocus AG (Karlsruhe, Germany). After that, the side surface was turned to remove the roughness and edge porosity, which allowed to determine the sample density by measuring the dimensions with an outside micrometer Micromar 40 ER from Mahr GmbH (Göttingen, Germany) and the weight with an XSR204 precision balance from Mettler Toledo GmbH (Greifensee, Switzerland). At least one microsection of each powder condition and scan speed was prepared. With ImageJ, the number and total area of hydrogen pores were analyzed. Hydrogen pores are hereafter defined as pores with a diameter below 3 µm.

3. Results

As described in the literature, the achievable sample density decreases with increasing powder moisture content of the analyzed powders before drying, Figure 1.

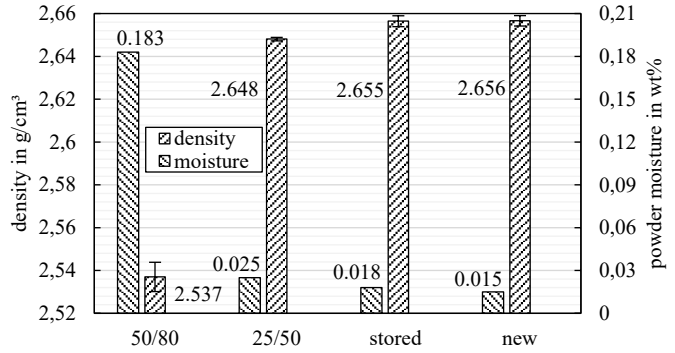

Figure 1: Influence of the different powder moisture conditions on the resulting sample density without drying. Scan velocity: 1150 mm/s.

The efficiency of the various drying methods is best seen with the most moisturized powder condition 50/80, Figure 2. Furnace drying can only slightly reduce the powder moisture content within an hour, even at the highest temperature of 200 °C. Vacuum drying is more efficient. The improved powder drying with a higher number of cycles (V20) is attributed to the more frequent inlet of fresh inert gas, which causes the powder in the bottle to swirl repeatedly. This allows the vaporized water to escape more efficiently as it does not have to diffuse through the powder. In-process laser drying is best at reducing powder moisture and the effect increases with increasing energy density E_v. When the effect of vacuum drying or in-process drying on the other powder states is considered, no effect can be measured.

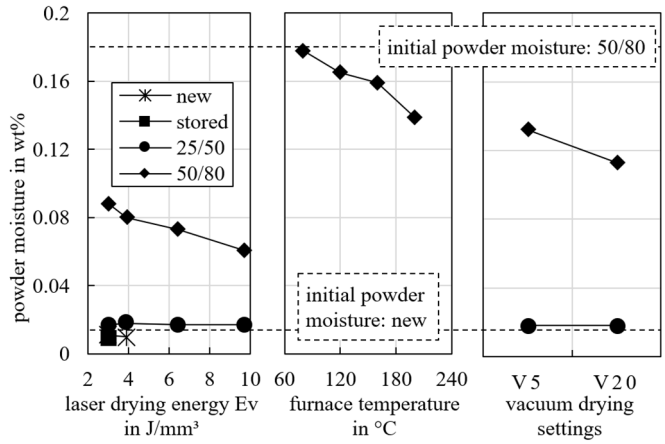

Figure 2: Influence of the different drying methods on the resulting powder moisture.

3.1. Furnace drying

The analysis of the sample density manufactured with furnace-dried powder shows that the density decreases despite decreasing powder moisture, Figure 4, as more LoF pores are forming. It can also be seen that a reduction in the scanning velocity results in less LoF pores, Figure 3,4.

The decreasing density at higher scan velocities could be attributed to an oxide layer growing on the powder particles during furnace drying with increasing furnace temperature because the oxygen from the bonded moisture on the particle surface is converted. Yang et al. proved that the temperature and time required to melt powder particles increases with increasing oxide layer thickness and that the oxides are partly not dissolved in the melt [14]. Therefore, increasing oxide layer thickness reduces the weld track width and depth at a constant energy input, favoring LoF pores. For this reason, a lower scanning speed positively affects the part density. The laser power acts longer on one increment of the melt path vector, which increases the melt pool geometry again. Therefore, the LoF pores become less and smaller, Figure 3.

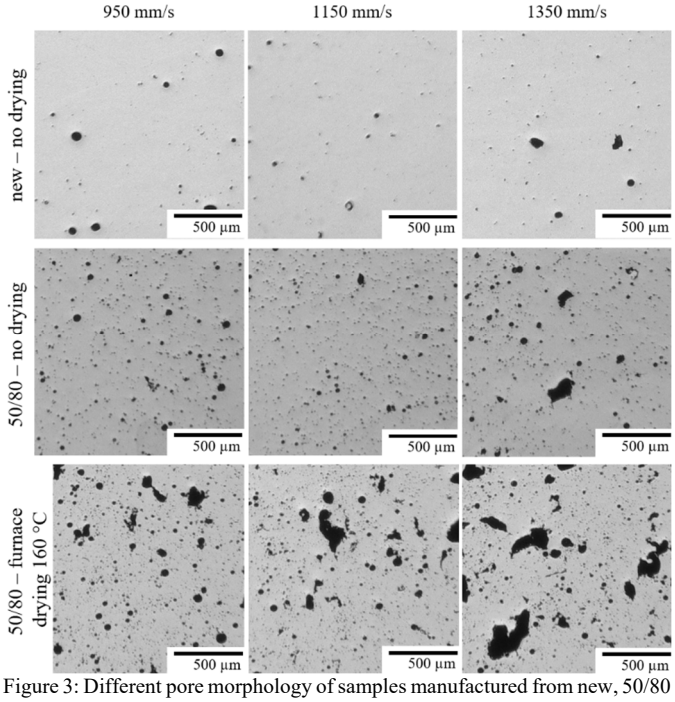

Figure 3: Different pore morphology of samples manufactured from new, 50/80 powder and 160 °C furnace-dried 50/80 powder at different scan velocities

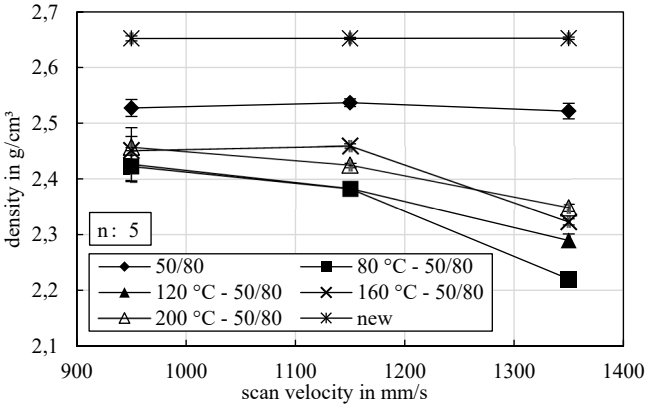

Figure 4: Influence of the scan velocity and the furnace drying temperature on the sample density produced with 50/80 powder and furnace-dried 50/80 powder. New powder not dried is shown for comparison. Error bars indicate the standard deviation.

The lower sample density made from 50/80 powder compared to new powder is not solely attributed to the formation of hydrogen pores. The size of the spherical pores appears to be too large, which is why process pores are assumed. It is assumed that the vaporization of the water, when

superheated by the laser, ejects particles from the layer. This leads to a lower powder layer density, resulting in a partial double exposure of the solidified layer, favoring process pores, Figures 3 and 4.

3.2. Vacuum drying

The sample density and pore morphology manufactured from vacuum-dried 50/80 powders show a similar trend to furnace drying. The samples from vacuum-dried 50/80 powder also have an overall lower density than those from undried 50/80 powder, Figure 5. The amount of LoF pores decreases with decreasing scanning velocity, compare Figure 3.

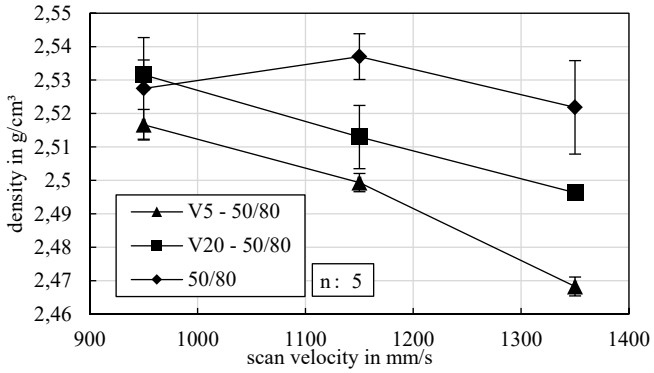

Figure 5: Influence of the scan velocity and the different vacuum drying cycles on the sample density of 50/80 powder and 50/80 vacuum-dried powders. Error bars indicate the standard deviation.

Vacuum drying has no reaction temperature that enables rapid oxidation during the vacuum drying time. Therefore, it is assumed that the vaporised moisture from the powder particles in a vacuum has a high reactivity, e.g., due to the formation of free hydrogen and oxygen radicals [15]. The moisture is continuously removed by flooding the bottle with fresh inert gas, so the possible reaction mass decreases, leading to a continuously decreased oxidation reaction. This results in the same measured moisture content of the 50/80 powder after V5 vacuum drying and 200°C oven drying, Figure 2. However, the oxide layer of the powder particles is probably thinner, so the sample density from vacuum-dried powder is higher than that from oven-dried powder. The lower density of V5 compared to V20 is attributed to less moisture removal and a longer vacuum retention time, leading to stronger oxide layer growth.

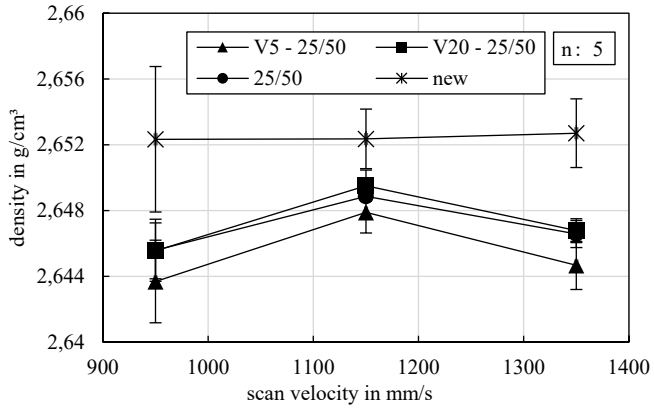

Figure 6: Influence of the scan velocity and the different vacuum drying cycles on the sample density of 25/50 powder and 25/50 vacuum-dried powders. Error bars indicate the standard deviation.

Samples produced from 25/50 or 25/50 vacuum-dried powders show no change in density. The density remains constant and is minimally lower than that of samples made from new powder, Figure 6. The pore morphology is similar to that when using new powder, Figure 2.

3.3. In-process laser drying

All produced laser-dried samples, regardless of the used powder condition, reach their maximum density at a scanning velocity of 1150 mm/s, so only these results are compared below, Figure 7.

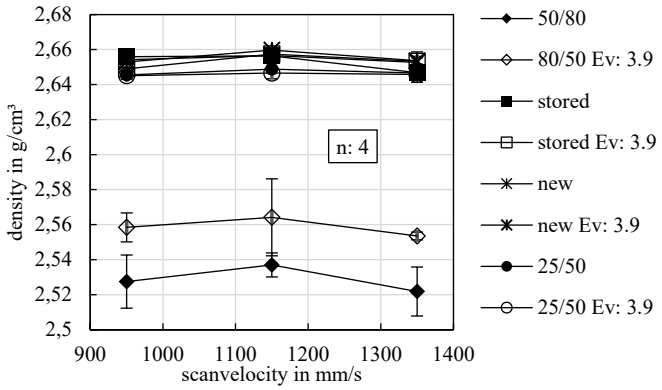

Figure 7: Influence of the scan velocity and laser drying energy of 3.9 J/mm³ on the sample density manufactured from new, stored, 25/50 and 50/80 powder. Error bars indicate the standard deviation.

The effect of laser drying is most evident when analyzing 50/80 powder. Drying energies up to 3.9 J/mm³ increase the density of the samples by up to 1.97 %, Figure 8. The evaluation of the microsections shows that fewer process pores but more LoF pores occur with increasing energy densities of the laser drying process, Figure 9. Like vaporized metal ejects particles from the powder bed during the melting process [16], the same effect is assumed when water is vaporized. It is assumed that a higher energy during drying causes a large number of particles to be ejected from the powder layer as the moisture evaporates quicker, which is why a proper component build-up is no longer possible with high drying energies. The amount of hydrogen pores reduces significantly from 28 % for undried powder to 9 % for laser-dried powder with an energy density of 3.9 J/mm³.At the highest drying energy of 9.6 J/mm³, a concentration of only 3 % is measured. However, it is doubtful whether the hydrogen pore measurement is valid due to the superposition with a high LoF porosity at the highest drying energy, Figure 8. An influence of laser drying on the samples from the other powder conditions is not evident.

At a drying energy density above 3.9 J/mm³, new, stored or 25/50 powder particles are sintering together. Due to the exposure area offset for drying in relation to the actual sample diameter, the surface roughness increases significantly, Figure 10. The sintering forms a coherent, brittle powder layer that does not adhere to the underlying layer. For this reason, the powder moisture analysis of high energy in-process drying was impossible because the coherently sintered layer was captured by the recoater and pushed away. The formation of a coherent layer was not observed at 50/80 powder.

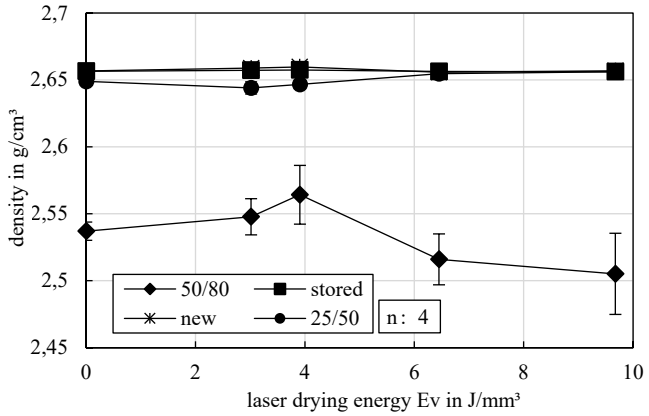

Figure 8: Influence of the laser drying energy on the sample density of all powder conditions for a scan velocity of 1150 mm/s. Error bars indicate the standard deviation.

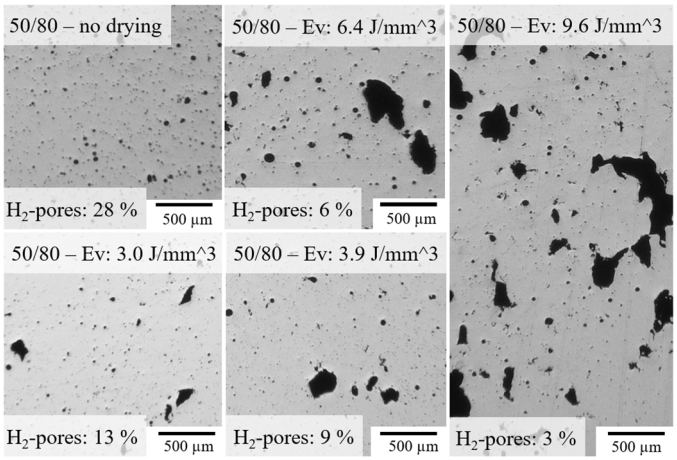

Figure 9: Different pore morphology of samples manufactured from 50/80 powder in-process dried with different energies. Scan velocity: 1150 mm/s

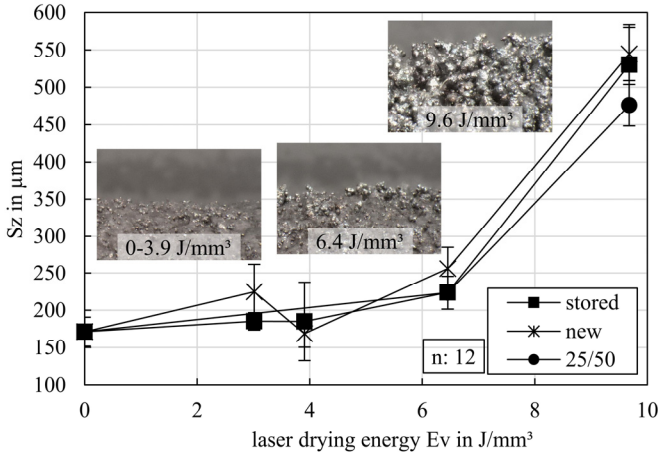

Figure 10: Influence of the drying energy on the sample surface roughness manufactured with different powder conditions. Error bars indicate the standard deviation.

4. Conclusion

If AlSi10Mg powder is moistened, the achievable component density decreases. The highest density of 2.65±0.002 g/cm³ is achieved using new powder with a moisture content of 0.015 wt% measured in the KFT. The active moistening of new powder or the storage of this powder in bottles without a vacuum-sealed bag increases the powder moisture, and the achievable sample density decreases. This requires powder drying. For this reason, three different drying methods were presented and compared in this paper. The furnace, vacuum, and in-process laser drying of the surface to be exposed before the actual melting. The most important findings can be summarized as follows:

- The best way to reduce powder moisture is to use high energy during in-process drying. Furnace drying has the weakest reduction effect.
- Furnace and vacuum drying of powders with a high moisture content presumably leads to the growth of an oxide layer around the particles. The growth of this oxide layer further reduces the achievable sample density.
- Only in-process drying enables a reduction in moisture and hydrogen pores in samples. However, the drying energy must be set low to prevent the powder particles from sintering during drying.
- None of the drying methods could achieve a powder state that allows the production of samples with the same density as with new powder.

In follow-up investigations, high-speed images should be taken during PBF-LB processing and laser drying of differently moist powders to visualize the influence of the evaporating water on the powder bed. Furthermore, the oxide layer thickness and its change, e.g., by TEM lamellae of individual powder particles of the same size, should be prepared.

To summarize, moisture in highly oxidation-sensitive AlSi10Mg powder cannot be removed using the methods discussed. An oxide-removing chemical washing process would still be conceivable but probably more complex than realizing a permanently closed powder cycle in an inert atmosphere to prevent moist absorption.

5. Acknowledgements

The authors thank Johannes Lohn and his company AMproved GmbH for vacuum drying the AlSi10Mg powder samples for these investigations.

This Project is supported by the Federal Ministry for Economic Affairs and Climate Action (BMWK) based on a decision by the German Bundestag.

References

[1] Fiegl, T., Franke, M., Raza, A., Hryha, E., Körner, C., 2021. Effect of AlSi10Mg0.4 long-term reused powder in PBF-LB/M on the mechanical properties. Materials & Design 212 (3), 110176.

[2] Yang, K.V., Rometsch, P., Jarvis, T., Rao, J., Cao, S., Davies, C., Wu, X., 2018. Porosity formation mechanisms and fatigue response in Al-Si-Mg alloys made by selective laser melting. Materials Science and Engineering: A 712 (Part 2), 166–174.

[3] Bayat, M., Thanki, A., Mohanty, S., Witvrouw, A., Yang, S., Thorborg, J., Tiedje, N.S., Hattel, J.H., 2019. Keyhole-induced porosities in Laser-based Powder Bed Fusion (L-PBF) of Ti6Al4V: High-fidelity modelling and experimental validation. Additive Manufacturing 30 (1), 100835.

[4] Huang, Y., Fleming, T.G., Clark, S.J., Marussi, S., Fezzaa, K., Thiyagalingam, J., Leung, C.L.A., Lee, P.D., 2022. Keyhole fluctuation and pore formation mechanisms during laser powder bed fusion additive manufacturing. Nature communications 13 (1), 1170.

[5] Wang, L., Zhang, Y., Chia, H.Y., Yan, W., 2022. Mechanism of keyhole pore formation in metal additive manufacturing. npj Comput Mater 8 (1), 3370–3379.

[6] Aboulkhair, N.T., Everitt, N.M., Ashcroft, I., Tuck, C., 2014. Reducing

porosity in AlSi10Mg parts processed by selective laser melting. Additive Manufacturing 1-4, 77–86.
[7] Limbasiya, N., Jain, A., Soni, H., Wankhede, V., Krolczyk, G., Sahlot, P., 2022. A comprehensive review on the effect of process parameters and post-process treatments on microstructure and mechanical properties of selective laser melting of AlSi10Mg. Journal of Materials Research and Technology 21, 1141–1176.
[8] Weiss, C., Heslenfeld, J., Saewe, J.K., Bremen, S., Häfner, C.L., 2022. Investigation on the influence of powder humidity in Laser Powder Bed Fusion (LPBF). Procedia CIRP 111, 115–120.
[9] Li, X.P., O'Donnell, K.M., Sercombe, T.B., 2016. Selective laser melting of Al-12Si alloy: Enhanced densification via powder drying. Additive Manufacturing 10, 10–14.
[10] Weingarten, C., Buchbinder, D., Pirch, N., Meiners, W., Wissenbach, K., Poprawe, R., 2015. Formation and reduction of hydrogen porosity during selective laser melting of AlSi10Mg. Journal of Materials Processing Technology 221 (2), 112–120.
[11] Cordova, L., Bor, T., Smit, M. de, Campos, M., Tinga, T., 2020. Measuring the spreadability of pre-treated and moisturized powders for laser powder bed fusion. Additive Manufacturing 32, 101082.
[12] Hartmüller, J., Ripperger, S., 2014. Calculation of Powder Particle Adhesion on Structured Surfaces. Chemie Ingenieur Technik 86 (8), 1260–1268.
[13] Grigull, U., Straub, J., Schiebener, P., 1984. Steam Tables in SI-Units/Wasserdampftafeln. Springer Berlin Heidelberg, Berlin, Heidelberg.
[14] Yang, X., Gao, F., Tang, F., Hao, X., Li, Z., 2021. Effect of Surface Oxides on the Melting and Solidification of 316L Stainless Steel Powder for Additive Manufacturing. Metall Mater Trans A 52 (10), 4518–4532.
[15] 2006. Principles of mass spectrometry applied to biomolecules. Wiley-Interscience, Hoboken, N.J., 687 pp.
[16] Yin, J., Wang, D., Yang, L., Wei, H., Dong, P., Ke, L., Wang, G., Zhu, H., Zeng, X., 2020. Correlation between forming quality and spatter dynamics in laser powder bed fusion. Additive Manufacturing 31, 100958.